JOURNAL OF MATERIALS SCIENCE 18 (1983) 3230–3242

Effect of alumina and monoclinic zirconia on the electrical conductivity of Sc_2O_3–ZrO_2 compositions

S. P. S. BADWAL
CSIRO Division of Materials Science, Advanced Materials Laboratory, PO Box 4331, Melbourne, Victoria, Australia 3001

Electrical conductivity measurements over the temperature range 400 to 1000° C have been made on specimens in the Sc_2O_3–ZrO_2–Al_2O_3 system as functions of Sc_2O_3 and Al_2O_3 contents. Both 4-probe d.c. conductivity and complex impedance dispersion analysis techniques were used. Samples which contained monoclinic ZrO_2 showed jumps and hysteresis effects, although these effects were considerably masked in alumina-rich samples. Conductivity results indicate that, in samples which contained relatively small amounts of Al_2O_3 (2 to 5 wt%) or were free from Al_2O_3, a significant proportion of the monoclinic ZrO_2 was present in series with the conduction paths of the oxygen ion vacancies. In Al_2O_3-rich samples the major proportion of monoclinic ZrO_2 appears to be preferentially distributed at locations in the microstructure where it had less influence on the conductivity. For samples which did not show jumps or hysteresis effects the Arrhenius plots had lower slopes at higher temperatures.

1. Introduction

Oxygen sensors based on O^{2-} conducting solid electrolyte membranes are widely used to measure, monitor and control oxygen [1–3] in the chemical and metallurgical industries. Typical applications include atmosphere control in heat treatment furnaces, combustion control for fuel economy and reduced emissions and process control in the metallurgical industry. These applications cover a wide range of atmospheres and temperatures.

An intermediate temperature range (400 to 700° C) oxygen sensor is currently under development in our laboratory [4]. The sensor is based on the principle of a differential oxygen probe and is similar in construction to our high temperature range (700 to 1300° C) sensor [5]. In the former sensor a solid electrolyte disc is welded onto an alumina tube of the required length and diameter by a high temperature eutectic welding operation. These sensors are rugged in construction, have low leak rates and, unlike zirconia tubes, are far less susceptible to thermal and mechanical shocks. However, for successful operation of the sensor over a period of time, the thermal expansion mismatch between the solid electrolyte disc and the alumina tube should be a minimum.

Thermal expansion coefficient measurements, leak rate tests and acoustic emission experiments on several compositions in the Sc_2O_3–ZrO_2–Al_2O_3 system [6] indicate that the 4.7 mol% Sc_2O_3–ZrO_2 composition containing 50 wt% Al_2O_3 is most suitable for this application. Alumina is added to increase the mechanical strength of the electrolyte matrix and to reduce the thermal expansion mismatch between the electrolyte and the alumina tube. This is essential to minimize cracking of the electrolyte and the alumina tube during preparation and subsequent thermal cycling of the sensor. The electrolyte also contains a small amount (4 to 15 wt%) of monoclinic ZrO_2 (unreacted and/or precipitated out during cooling). The way in which the insulating alumina and m-ZrO_2 (monoclinic ZrO_2) phases are distributed in the conducting phase can have a significant effect on the electrical conductivity of the solid electrolyte and thus on the sensor performance at lower temperatures.

0022–2461/83 $03.00 + .12

Although investigations into the conductivity of some compositions of the Sc_2O_3–ZrO_2 system have been carried out before [7–11], the effect of m-ZrO_2 (a phase present for low Sc_2O_3 concentrations) on the conductivity has not yet been fully elucidated. No conductivity data is available for the Sc_2O_3–ZrO_2–Al_2O_3 system except a brief report from this laboratory [12]. In order to ascertain the role of alumina and monclinic ZrO_2 on the electrical conductivity, several samples of Sc_2O_3–ZrO_2–Al_2O_3 containing varying amounts of alumina (up to a maximum of 50 wt %) and Sc_2O_3 (4 to 8 mol %) were prepared.

Both 4-probe d.c. and 2-probe complex impedance dispersion analysis techniques have been used to measure their electrical conductivities. The distribution of phases was examined with optical and scanning electron microscopes. Dilatometry curves were obtained for several samples to study phase transformations.

2. Experimental details

The materials used in the preparation of various samples were: ZrO_2 containing 2 wt % HfO_2 (Harshaw, > 99.5%, LOI (Loss on Ignition) = 0.84%), Sc_2O_3 (AMDEL Australia, 99.5%, LOI = 0.94 wt %), Al_2O_3 (Reynolds, 99.7%, LOI = 0.84%).

Two series of samples were prepared. In "Series A" the concentration of Al_2O_3 was kept constant at 50 wt % while the composition of Sc_2O_3–ZrO_2 was varied between 4 and 8 mol % Sc_2O_3. In "Series B" the composition of Sc_2O_3–ZrO_2 was kept constant at 5.9 mol % Sc_2O_3 and the alumina concentration was varied between 0 and 50 wt %. The bars of various samples for conductivity measurements were prepared as follows: ZrO_2, Sc_2O_3 and Al_2O_3 powders, in the required proportion, were mixed thoroughly and calcined at 1100° C for one hour. The mixture after addition of approximately 5 wt % water was compacted into bars at a low pressure. These were then isostatically pressed at a pressure of 205 MN m^{-2} followed by sintering at 1700° C for 15 h in air in a molybdenum wire wound furnace. Some samples were given a further heat treatment in a gas fired furnace. Details of heat treatments are given in Table I.

The experimental techniques have been described elsewhere [13]. In brief, the samples for 4-probe conductivity measurements were 20 to 30 mm long and had a diameter between 5 and 7 mm. The 4-probe d.c. technique involved passing a constant current of 0.5 to 300 μA (depending on the specimen resistance) from a constant current source through the two outer electrodes and measuring the potential drop across the two inner electrodes with an electrometer (input impedance $> 10^{14}\,\Omega$). Measurements were made at 25° C temperature intervals during several heating and cooling cycles over the range 400 to 1000° C. After a temperature change, sufficient time (45 to 60 min) was given for thermal equilibrium conditions to re-establish.

Complex impedance measurements were made on two representative compositions, namely, samples A7 and B3 with a Solartron frequency response analyser 1174 (frequency range 0.1 Hz to 1 MHz) over the temperature range 350 to 700° C in air. Samples for these measurements were 2 to 4 mm long, had a diameter between 5 and 7 mm and contained platinum paste electrodes.

X-ray diffraction patterns of sintered discs from all the samples were taken with a Rigaku diffractometer using Cu$K\alpha$ radiation. The m-ZrO_2 content in various specimens was measured by the integrated intensity method described by Garvie and Nicholson [14] (Table I). Dilatometry curves were recorded on several samples at a typical heating and cooling rate of 300° C h^{-1}. However, slower cooling rates (35 to 40° C h^{-1}) were used for some samples. The microstructure of polished surfaces of various samples was examined with optical and scanning electron microscopes.

3. Results and discussion

3.1. X-ray studies

The X-ray diffraction patterns of Al_2O_3-containing samples with Sc_2O_3 concentration $\geqslant$ 5.9 mol % showed the presence of only alumina and a tetragonal phase [15]. In the diffraction patterns of the 2 and 5 wt % Al_2O_3 samples there were also m-ZrO_2 lines (only traces in 5 wt % Al_2O_3 samples). All Sc_2O_3–ZrO_2 samples and those in the Sc_2O_3–ZrO_2–Al_2O_3 system with Sc_2O_3 concentration $\leqslant$ 4.9 mol % contained significant proportions of m-ZrO_2. The m-ZrO_2 content decreased with higher temperature treatment and increased with decreased scandia concentration (Table I). More significantly, the presence of alumina had the effect of decreasing the m-ZrO_2 content in the specimens considerably. For example, 5.9 mol % Sc_2O_3–ZrO_2 and 98 wt % (5.9 mol % Sc_2O_3–ZrO_2) + 2 wt % Al_2O_3 samples prepared under

TABLE I Preparation details and activation energies of various samples

Specimen	Specimen starting composition	Heat treatment T (°C) (h)	Monoclinic§ ZrO_2 (wt %)	Activation energy (kJ mol^{-1})	
				High temperature region	Low temperature region
A1	50 wt % (3.9 mol % Sc_2O_3–ZrO_2) + 50 wt % Al_2O_3	1700(15)	36	79 ± 2	116 ± 3
A2	50 wt % (4.4 mol % Sc_2O_3–ZrO_2) + 50 wt % Al_2O_3	1700(15)	28	74 ± 2	104 ± 5
A3	50 wt % (4.7 mol % Sc_2O_3–ZrO_2) + 50 wt % Al_2O_3	1700(15)	15	92 ± 3	110 ± 3
A4	50 wt % (4.7 mol % Sc_2O_3–ZrO_2) + 50 wt % Al_2O_3	1700(15), 1800(0.3)	~ 6	82 ± 3	106 ± 3
A5	50 wt % (4.9 mol % Sc_2O_3–ZrO_2) + 50 wt % Al_2O_3	1700(15)	13	77 ± 3	110 ± 3
A6	50 wt % (5.9 mol % Sc_2O_3–ZrO_2) + 50 wt % Al_2O_3	1700(15)	*	67 ± 4†	109 ± 4†
A7	50 wt % (6.8 mol % Sc_2O_3–ZrO_2) + 50 wt % Al_2O_3	1700(15)	*	67 ± 4†	115 ± 4†
A7	50 wt % (6.8 mol % Sc_2O_3–ZrO_2) + 50 wt % Al_2O_3	1700(15)	*	–	112 ± 5¶
A8	50 wt % (7.8 mol % Sc_2O_3–ZrO_2) + 50 wt % Al_2O_3	1700(15)		78 ± 2†	127 ± 4†
B1	5.9 mol % Sc_2O_3–ZrO_2	1700(15)	27	75 ± 3	120 ± 3
B2	5.9 mol % Sc_2O_3–ZrO_2	1700(15), 1900(3)	17	77 ± 2	115 ± 3
B3	5.9 mol % Sc_2O_3–ZrO_2	1700(15), 1900(3) 1900(2.5)‡	11	77 ± 2	111 ± 3
B3	5.9 mol % Sc_2O_3–ZrO_2	1700(15), 1900(3) 1900(2.5)‡	11	–	100 ± 6¶
B4	98 wt % (5.9 mol % Sc_2O_3–ZrO_2) + 2 wt % Al_2O_3	1700(15)	~ 5	88 ± 2	106 ± 3
B5	95 wt % (5.9 mol % Sc_2O_3–ZrO_2) + 5 wt % Al_2O_3	1700(15)	Traces	86 ± 2	103 ± 3
B6	90 wt % (5.9 mol % Sc_2O_3–ZrO_2) + 10 wt % Al_2O_3	1700(15)	*	66 ± 3†	109 ± 3†
B7	80 wt % (5.9 mol % Sc_2O_3–ZrO_2) + 20 wt % Al_2O_3	1700(15)	*	69 ± 4†	110 ± 3†
B8	70 wt % (5.9 mol % Sc_2O_3–ZrO_2) + 30 wt % Al_2O_3	1700(15)	*	70 ± 4†	109 ± 4†
B9	60 wt % (5.9 mol % Sc_2O_3–ZrO_2) + 40 wt % Al_2O_3	1700(15)	*	72 ± 4†	111 ± 4†
B10	50 wt % (5.9 mol % Sc_2O_3–ZrO_2) + 50 wt % Al_2O_3	1700(15)	*	67 ± 4†	109 ± 4†

*X-ray diffraction patterns of these samples do not show the presence of monoclinic ZrO_2 lines.
†Activation energies determined by fitting the data to Equation 1.
‡Sample was air quenched after third firing at 1900° C for 2.5 h.
§Errors in the estimation of m-ZrO_2 are typically ± 10% of the measured m-ZrO_2 content.
¶From complex impedance dispersion analysis.
The data for samples A3 and A4 from [12].

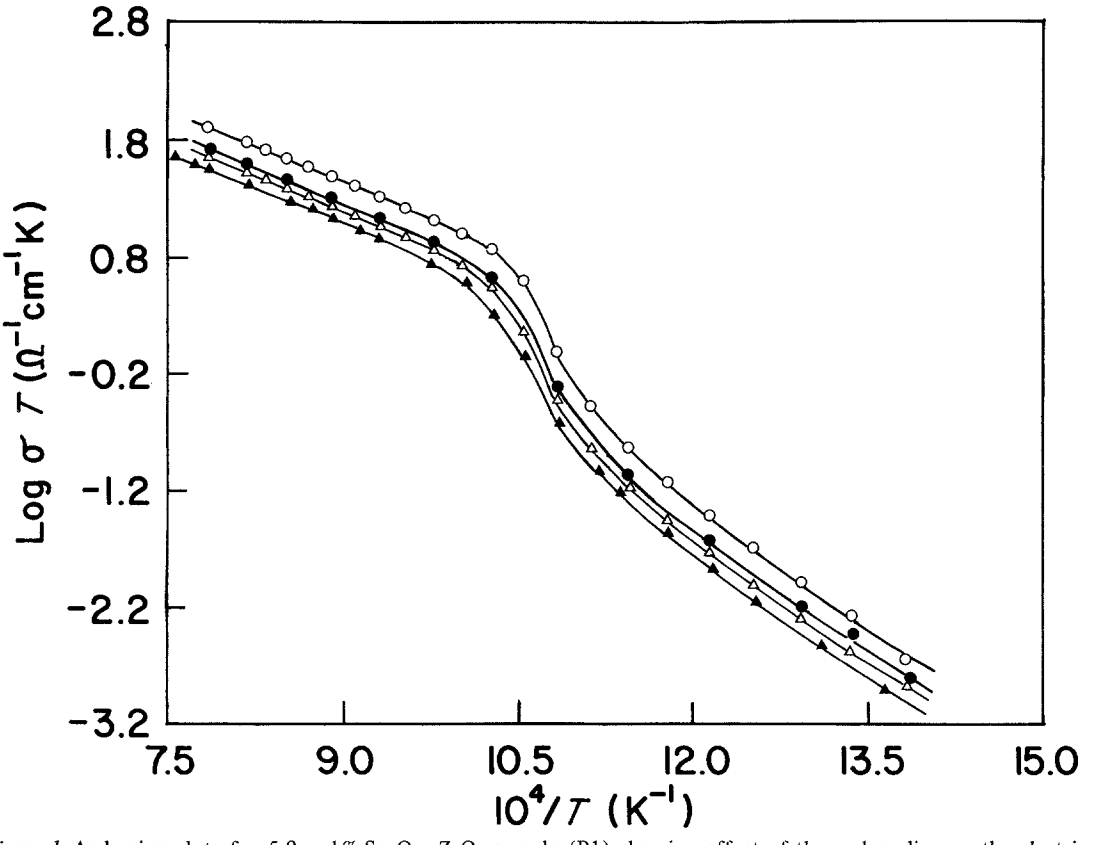

Figure 1 Arrhenius plots for 5.9 mol% Sc_2O_3–ZrO_2 sample (B1) showing effect of thermal cycling on the electrical conductivity. ○–1st, ●–2nd, △–3rd and ▲–4th cooling cycle.

identical conditions contained grossly different amounts of m-ZrO_2, namely 27 and 5 wt% respectively. It is surprising that the presence of a mere 2 wt% Al_2O_3 should have such a large effect. Phase equilibrium studies [15] show that alumina dissolves sparingly in the Sc_2O_3–ZrO_2 fluorite solid solutions, and only marginally lowers the Sc_2O_3 concentration at the low-Sc_2O_3 boundary of the fluorite field at 1800° C. The difference in m-ZrO_2 content between these two samples is therefore unlikely to be an equilibrium effect. The phase studies [15] also suggest that Al_2O_3 enhances the rate of the reaction between Sc_2O_3 and ZrO_2 powders, thus enabling equilibrium to be more readily achieved. It is likely that a difference in the reaction rate is responsible for the effect of Al_2O_3 on the m-ZrO_2 content observed in the present work. Such an explanation implies that the 27 wt% m-ZrO_2 in the 5.9 mol% Sc_2O_3–ZrO_2 specimen largely represents unreacted ZrO_2.

3.2. D.C. conductivity results

3.2.1. Effect of cycling

All the specimens showed time-dependent behaviour, resulting in 10 to 20% decrease in the conductivity, during the initial 20 to 30 h after they had been heated to 1000° C for the first time. This can be attributed to the thermal history of the samples, the effect of minor surface impurities, and ordering. On subsequent cycling the conductivity data was reproducible for various heating and cooling cycles within experimental errors ($< \pm 2\%$) except for those samples which showed jumps and hysteresis effects in the conductivity curves (see below). For the latter samples a degradation of the conductivity was observed on successive cycling (Fig. 1), although this effect was less pronounced in samples which contained a significant proportion of alumina. The progressive degradation of the conductivity in samples containing m-ZrO_2 was accompanied by mechanical weakening of the sintered body. Microscopic examination showed the formation of an extensive network of cracks after thermal cycling. Cracking is attributed to the volume change which accompanies the m-$ZrO_2 \rightleftharpoons$ t-ZrO_2 transformation (see below) and the cracks probably caused the reduction in conductivity. The disintegration of the specimens

was much less severe in series A, where the high volume fraction of Al_2O_3 (approximately 60% by volume) helped to hold the matrix together.

3.2.2. Jumps and hysteresis effects (conductivity and dilatometry curves)

Jumps and hysteresis effects in the conductivity curves were observed whenever m-ZrO_2 was detected by room temperature X-ray analysis. For example, these effects were observed in the conductivity curves for specimens from series A when the Sc_2O_3 concentration was $\leqslant 4.9$ mol% (Fig. 2). Similar behaviour was observed for all series B specimens which contained m-ZrO_2 (even in traces). The height of the jump appeared to be related to the gross m-ZrO_2 content. This is shown in Fig. 3 for three samples of 5.9 mol% Sc_2O_3–ZrO_2 composition which contained different amounts of m-ZrO_2 due to different heat treatments. Samples which contained m-ZrO_2 also showed inflection(s) in the thermal expansion curves corresponding to the m-$ZrO_2 \rightleftharpoons$ t-ZrO_2 transformation. These observations suggest that the jumps and the hysteresis effects in the Arrhenius plots were associated with the diffusionless m-$ZrO_2 \rightleftharpoons$ t-ZrO_2 transformation.

The temperature of the jump (T_{jump}), in general, was lower during the cooling cycle by 50 to 100° C than during the heating cycle. The T_{jump} decreased with increased Al_2O_3 content. For example during the cooling cycle, it was 700 to 710° C for samples B1 to B3, 670 to 680° C for sample B4, 650 to 655° C for sample B5 and 630 to 645° C for series A samples.

For series A samples jumps and hysteresis effects almost disappeared when the concentration of m-ZrO_2 was less than ~ 6 wt%. This is shown in Fig. 4a for two samples of 50 wt% (4.7 mol% Sc_2O_3–ZrO_2) + 50 wt% Al_2O_3 which

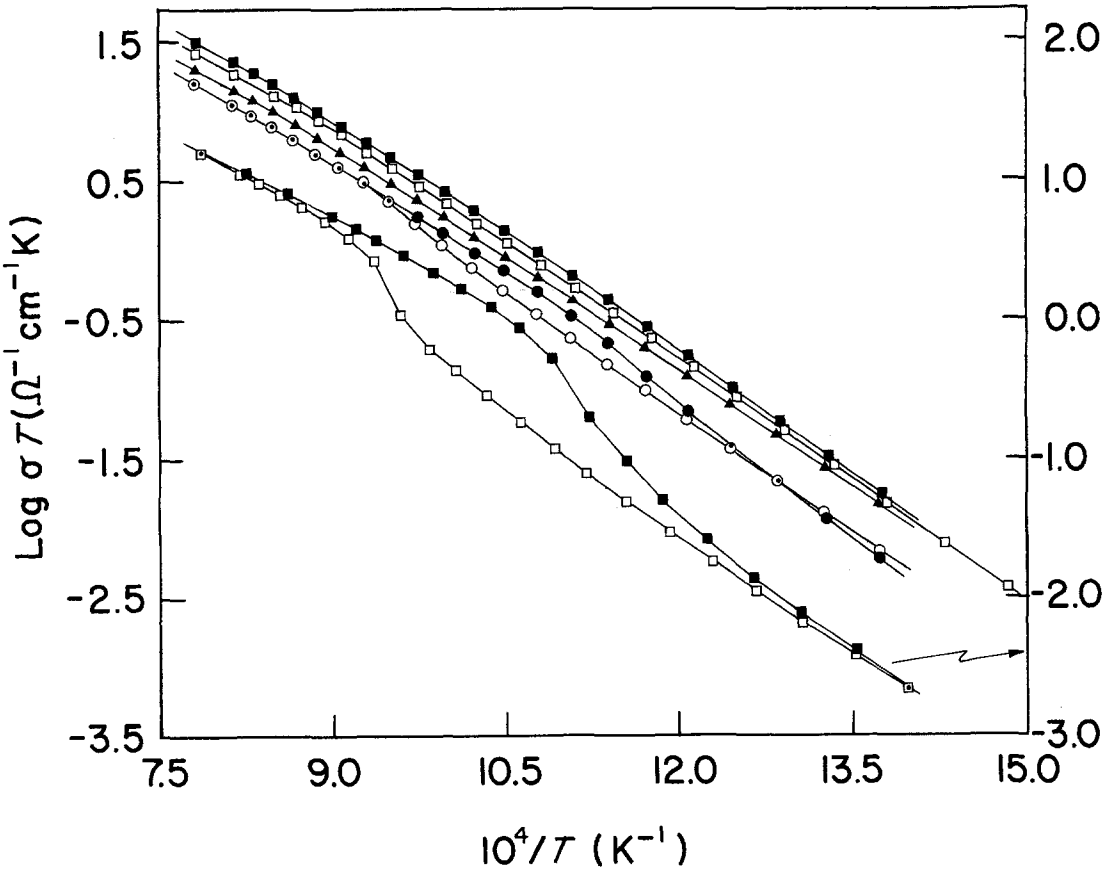

Figure 2 Arrhenius plots for series A samples containing 50 wt% Al_2O_3. ■–7.8 mol% Sc_2O_3–ZrO_2; □–6.8 mol% Sc_2O_3–ZrO_2; ▲–5.9 mol% Sc_2O_3–ZrO_2 (heating and cooling cycle data for these samples overlapped); ○–heating, ●–cooling cycle 4.7 mol% Sc_2O_3–ZrO_2; ▫–heating, ▪–cooling cycle 4.4 mol% Sc_2O_3–ZrO_2. The conductivity axis for the lower graph is on the right side.

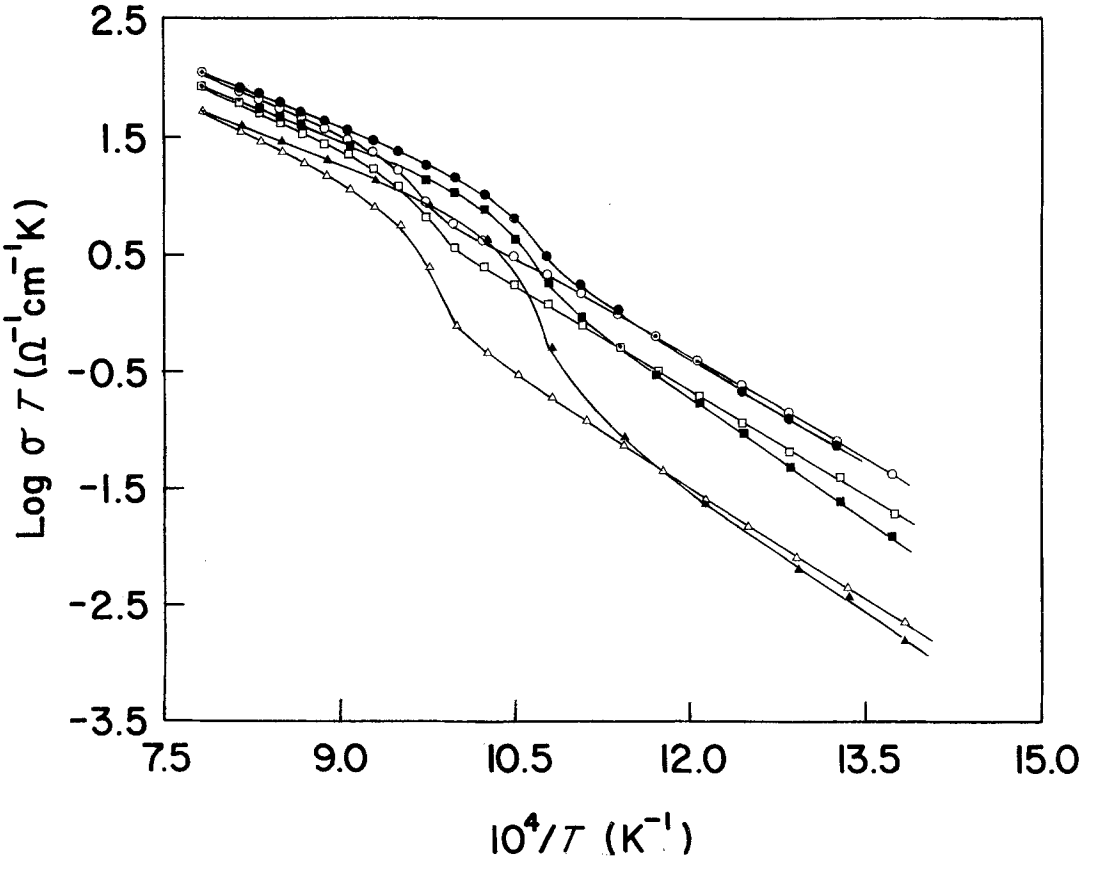

Figure 3 Arrhenius plots for 5.9 mol% Sc_2O_3–ZrO_2 composition showing the effect of m-ZrO_2 on the size of the hysteresis loop. Sample: B1 △–heating, ▲–cooling cycle; B2 □–heating, ■–cooling cycle; B3 ○–heating, ●–cooling cycle.

contained different amounts of m-ZrO_2 due to dissimilar heat treatments [12]. In other samples which contained small amounts of alumina (2 to 5 wt%) or were free of alumina, hysteresis effects occurred even for traces of m-ZrO_2 (Fig. 4b). Moreover, jumps in the conductivity curves were considerably more pronounced for series B samples compared with those of series A for similar amounts of m-ZrO_2 as can be seen by comparison of Figs. 2 to 4 and Table I. These observations suggest that for series A samples a significant proportion of the m-ZrO_2 was located preferentially at sites where it had little influence on the conductivity. On the other hand most of the m-ZrO_2 in series B samples was probably located at regions in the microstructure, for example in series with the conducting phase, where it could strongly influence the conductivity. Microstructural studies on these samples are in progress in our laboratory.

3.2.3. Conductivity as a function of Sc_2O_3 content

The results of 4-probe d.c. conductivity measurements as a function of Sc_2O_3 concentration and temperature, for series A specimens, are plotted in Fig. 2. These show a monotonic decrease in the conductivity with decrease in the Sc_2O_3 concentration down to 5.9 mol% Sc_2O_3. Hysteresis effects were observed below this Sc_2O_3 concentration. It should be pointed out here that in the pure Sc_2O_3–ZrO_2 system the maximum value of the conductivity was reported for a Sc_2O_3 concentration between 8 and 9 mol% [8].

3.2.4. Conductivity as a function of Al_2O_3 content

Arrhenius plots for 5.9 mol% Sc_2O_3–ZrO_2–Al_2O_3 as a function of alumina concentration are given in Fig. 5. The distribution of Al_2O_3 and Sc_2O_3–ZrO_2 phases is shown by SEM micrographs of the

polished surfaces of various samples in Fig. 6. Up to 30 wt % alumina, the Sc_2O_3–ZrO_2 phase was continuous with the alumina phase distributed in it. However, above 40 wt % Al_2O_3 the alumina phase also appeared to be continuous. For a two phase system consisting of a conductor and an insulator phase, three regions of different microstructure and conductivity can be recognized as the volume fraction of the insulator phase increases [16, 17].

(i) The insulator phase is discontinuously distributed in the continuous conductor phase.

(ii) A region where both phases are continuous.

(iii) The conductor phase is discontinuously distributed in the insulator phase.

In the first two cases the conductor phase will undoubtedly dominate the conductivity of the mixture, although the conductivity may not vary in direct proportion with the volume fraction of the conductor phase. Increased path length, isolation of certain grains of the conductor phase by the insulator phase, grain boundaries between the two phases, grain size, shape and distribution of both phases are some of the factors which determine the conductivity of the two phase mixture.

Plots of conductivity against volume fraction of the insulator phase* at several temperatures (Fig. 7) show a nonlinear decrease of conductivity with increased insulator content and indicate that the conductor phase was still continuous up to approximately 65 vol % of the insulator phase.

3.3. Complex impedance measurements

The results of complex impedance measurements for samples A7 and B3 are shown in Fig. 8. A single crystal electrolyte sample normally gives a perfect semicircular arc in the complex impedance plane, the arc intercepting the real axis vertically and having its centre on the real axis. The equiv-

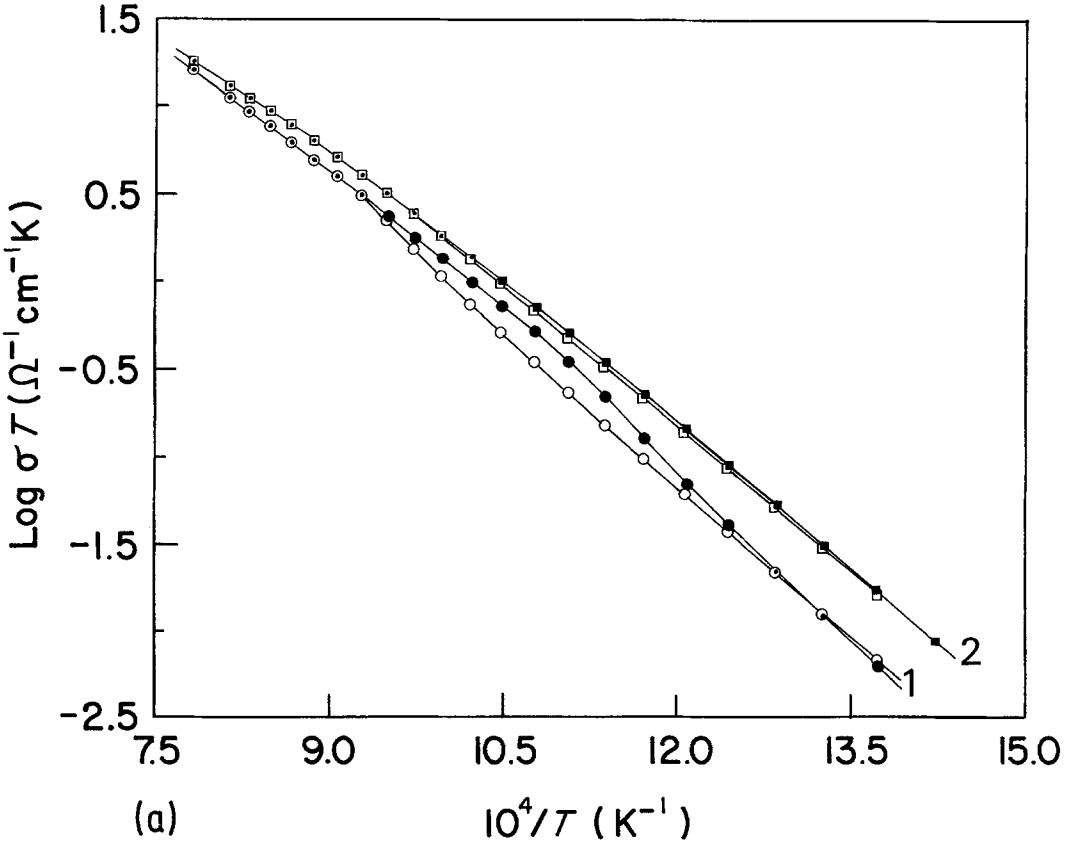

Figure 4 (a) Arrhenius plots for samples: A3 ○–heating, ●–cooling cycle; A4 □–heating, ■–cooling cycle. (b) Arrhenius plots for samples: B4 □–heating, ■–cooling cycle; B5 ○–heating, ●–cooling cycle.

*In determining the volume fraction of the insulator phase, both pores and alumina were taken into account (it is worth mentioning here that the porosity in these samples decreased with increase in the Al_2O_3 content).

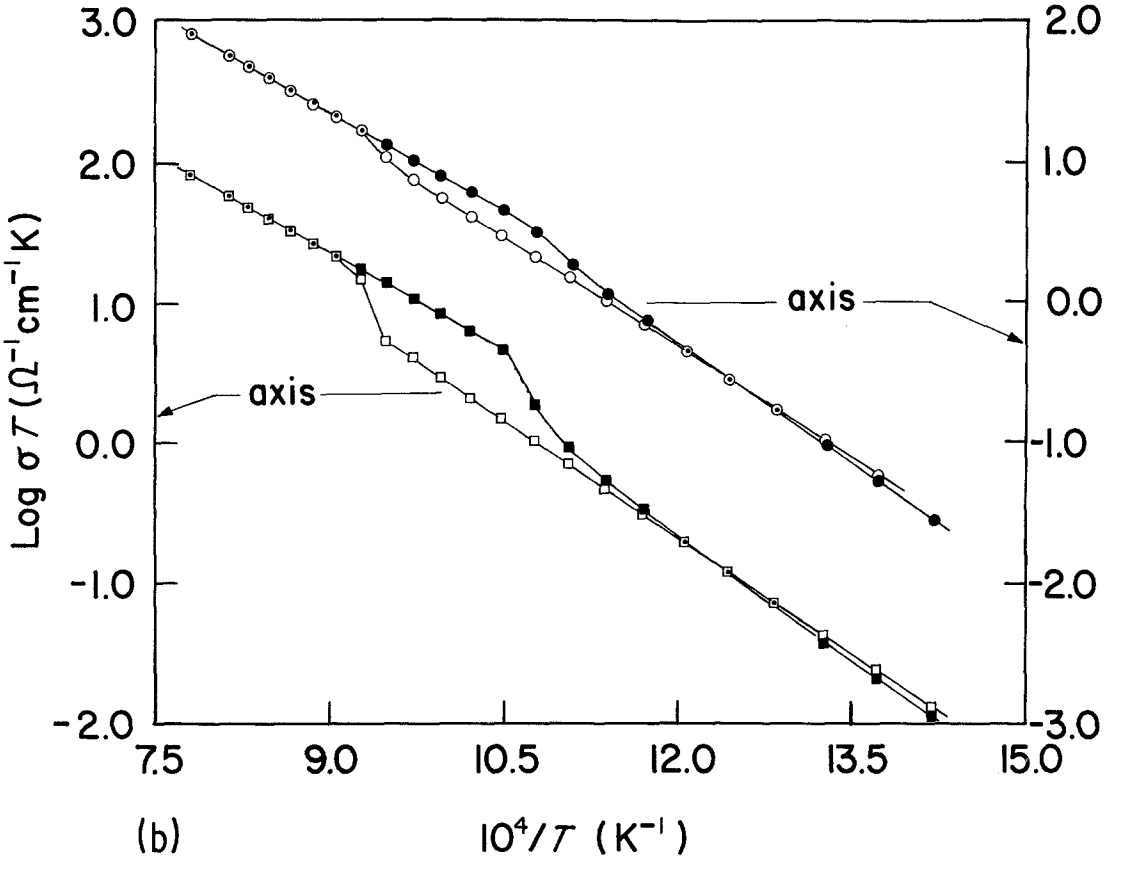

Figure 4 Continued

alent circuit for the arc is a resistor (the lattice resistance) in parallel with a capacitor (the geometric capacitance) [18]. In polycrystalline samples the behaviour is complicated by inhomogeneities and by grain boundaries, particularly if poorly conducting phases occur at grain boundaries. In such cases the partial or complete blocking of charge carriers at these locations can cause the build-up of space charge layers which produce another arc in the complex impedance plane. This additional arc is generally represented by a series network of several parallel resistor–capacitor combinations [19]. The resulting distribution of time constants causes the arc to be centred on a line which is depressed below the real axis, the angle of depression increasing with the spread of time constants.

In the present study each sample produced only one electrolyte arc over the temperature range 350 to 700° C. For neither sample was this arc a perfect semicircle. At the highest frequencies the data points approached the real axis vertically, indicating that at these frequencies the total impedance was dominated by the volume resistance of the grains. However, at low frequencies the data points could be represented by the Cole–Cole distribution of relaxation times [20] with an angle of depression of about 20°. These results suggest that, in each sample, there was considerable overlap between the volume resistance arc and the grain boundary arc with a distribution of time constants. This overlap made it impossible to separate the contributions of grain boundary and volume resistance, and served to emphasize the complicated nature of the conduction processes in these multiphase materials at low temperatures. The measurements were made below T_{jump} in the case of sample B3 and, for A7, below the temperature where a significant change in apparent activation energy occurs. Over the frequency range available to us, it was not possible to observe volume resistance arc at temperatures where the conduction process with low activation energy was dominant.

3.4. Activation energies for conduction mechanisms

For all samples from both series, which did not show jumps and hysteresis effects, a distinct

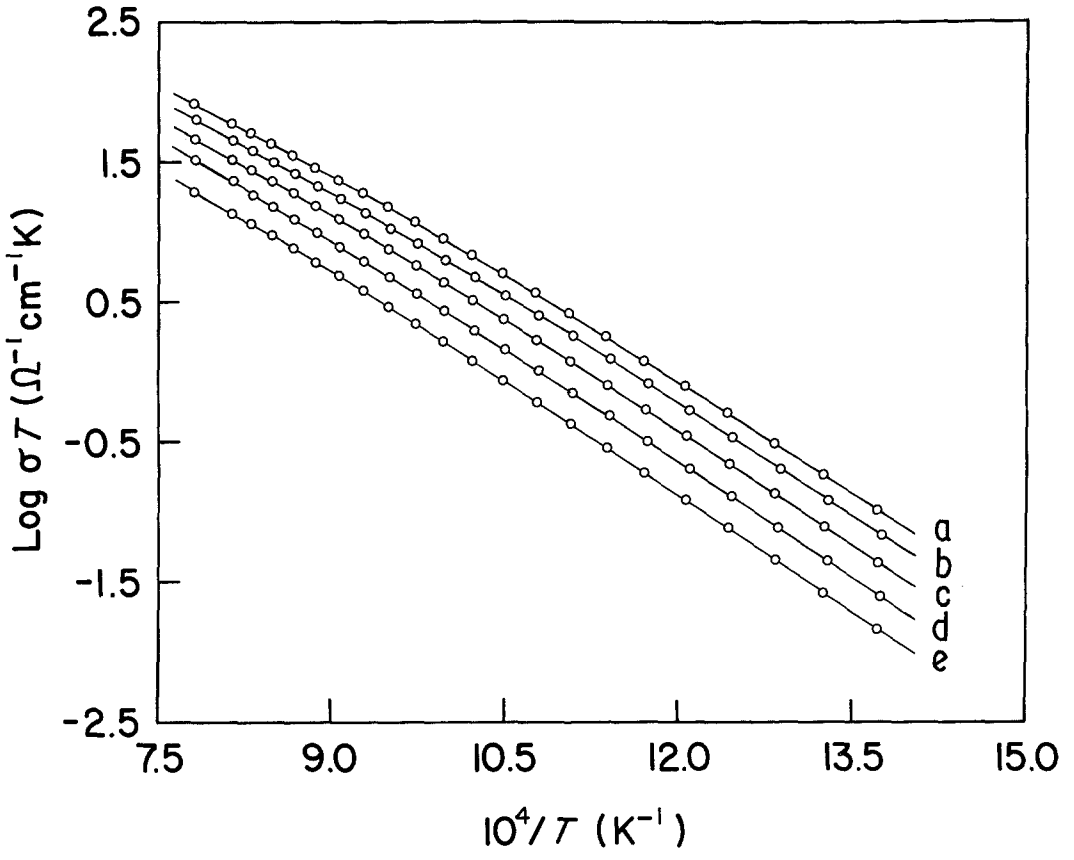

Figure 5 Arrhenius plots for 5.9 mol% Sc_2O_3–ZrO_2–Al_2O_3 samples as a function of Al_2O_3 concentration. Al_2O_3 wt %: (a) 10, (b) 20, (c) 30, (d) 40, (e) 50.

curvature in the Arrhenius plots was observed, the activation energy decreasing with increased temperature. The data were fitted to a relationship of the form [13]:

$$\rho = A_1 T \exp(E_1/RT) + A_2 T \exp(E_2/RT) \quad (1)$$

where ρ is the total resistivity, A_1 and A_2 are pre-exponential factors and E_1 and E_2 are activation energies. Equation 1 recognises contributions from two conducting processes in series, each with a different activation energy. For samples which showed hysteresis effects in the conductivity plots, the data could not be fitted to Equation 1 and the activation energy was calculated from a few data points at each end of the curve using the Arrhenius relation: $\rho = AT \exp(E/RT)$. The activation energy for the high temperature region was calculated using data from the cooling curve, and heating cycle data were used to determine the low temperature activation energy. All values are given in Table I.

The low activation energy process which dominates the conductivity behaviour at higher temperatures is attributed to dielectric polarization phenomena within the bulk of the grain due to the migration of the oxygen ion vacancies. The activation energy values for oxygen ion conduction in the bulk of the grain (high temperature region) compare well with the values reported in the literature for Sc_2O_3–ZrO_2 compositions [7, 13]. The activation energy values for samples B3 and A7 determined from complex impedance dispersion analyses of the electrolyte arc are similar to those obtained from the low temperature 4-probe d.c. conductivity data (Table I). The mechanism for this high activation energy process appears to be complex and has not been established yet, although a significant contribution from space charge phenomena at the grain boundaries is anticipated in these multiphase materials. The activation energy for the low temperature region can be influenced by the nature of the impurities and/or precipitated (or

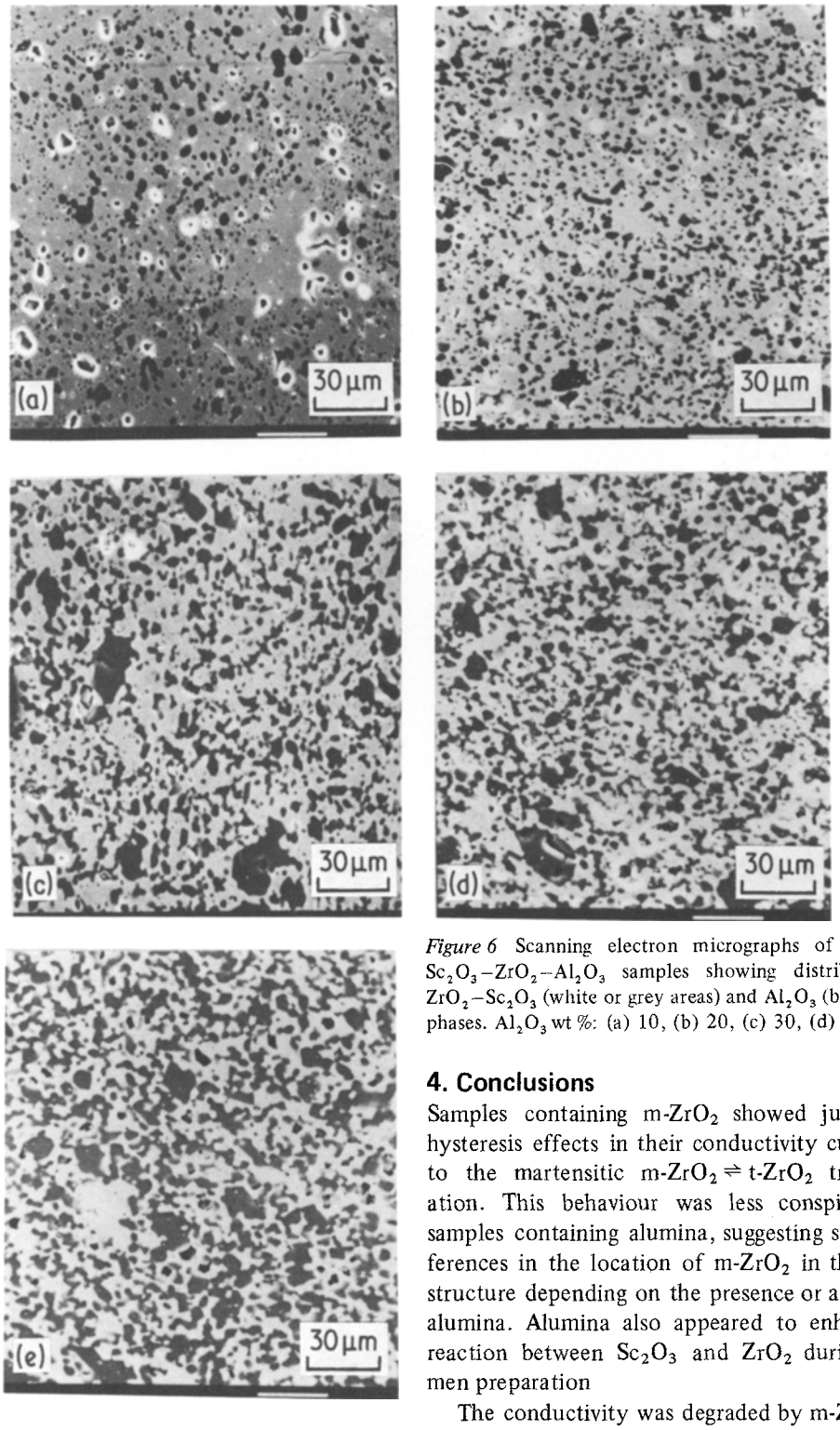

Figure 6 Scanning electron micrographs of 5.9 mol% Sc_2O_3–ZrO_2–Al_2O_3 samples showing distribution of ZrO_2–Sc_2O_3 (white or grey areas) and Al_2O_3 (black areas) phases. Al_2O_3 wt %: (a) 10, (b) 20, (c) 30, (d) 40, (e) 50.

unreacted) phases at the grain boundaries and trapping of the oxygen ion vacancies by the dopant cation as discussed in a previous publication [13].

4. Conclusions

Samples containing m-ZrO_2 showed jumps and hysteresis effects in their conductivity curves due to the martensitic m-$ZrO_2 \rightleftharpoons$ t-ZrO_2 transformation. This behaviour was less conspicuous in samples containing alumina, suggesting subtle differences in the location of m-ZrO_2 in the microstructure depending on the presence or absence of alumina. Alumina also appeared to enhance the reaction between Sc_2O_3 and ZrO_2 during specimen preparation

The conductivity was degraded by m-ZrO_2 and, in the absence of m-ZrO_2, by alumina, although in the latter case the conducting phase appeared still to be continuous down to a volume fraction of 0.35.

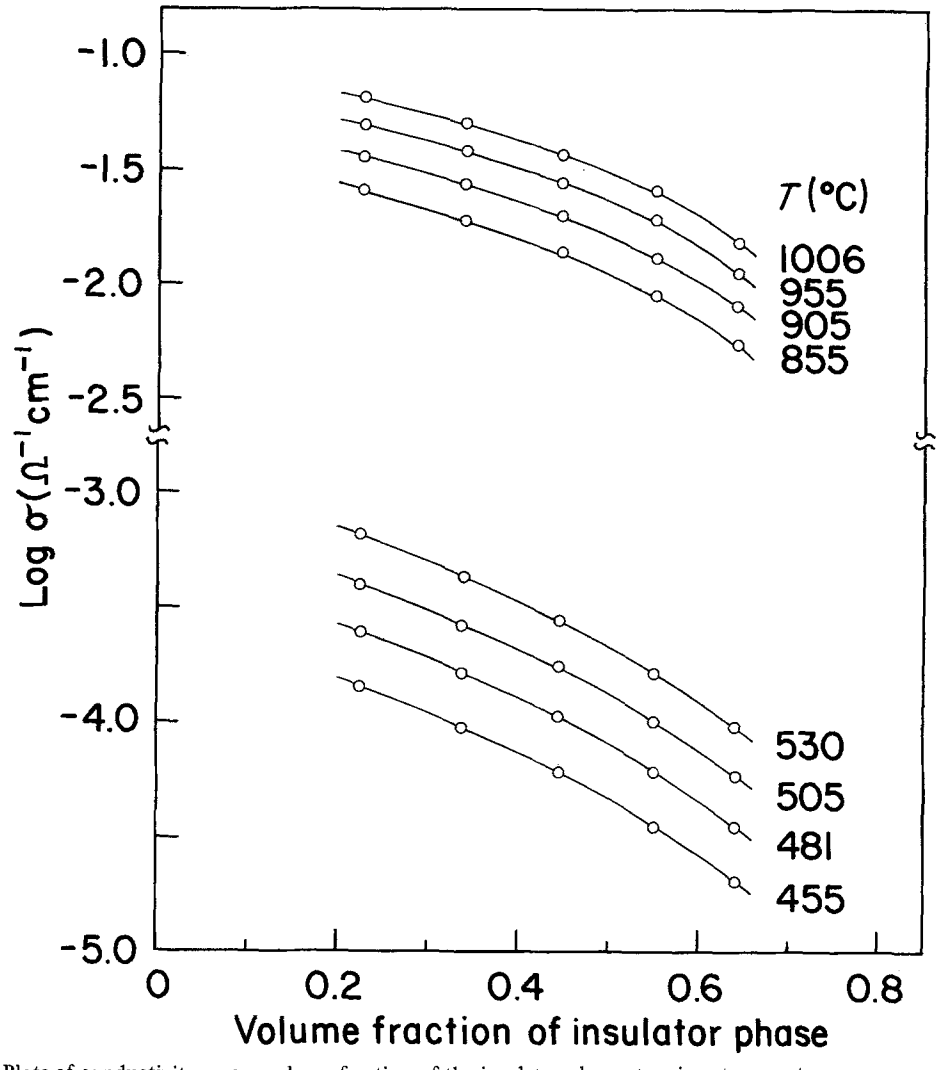

Figure 7 Plots of conductivity versus volume fraction of the insulator phase at various temperatures.

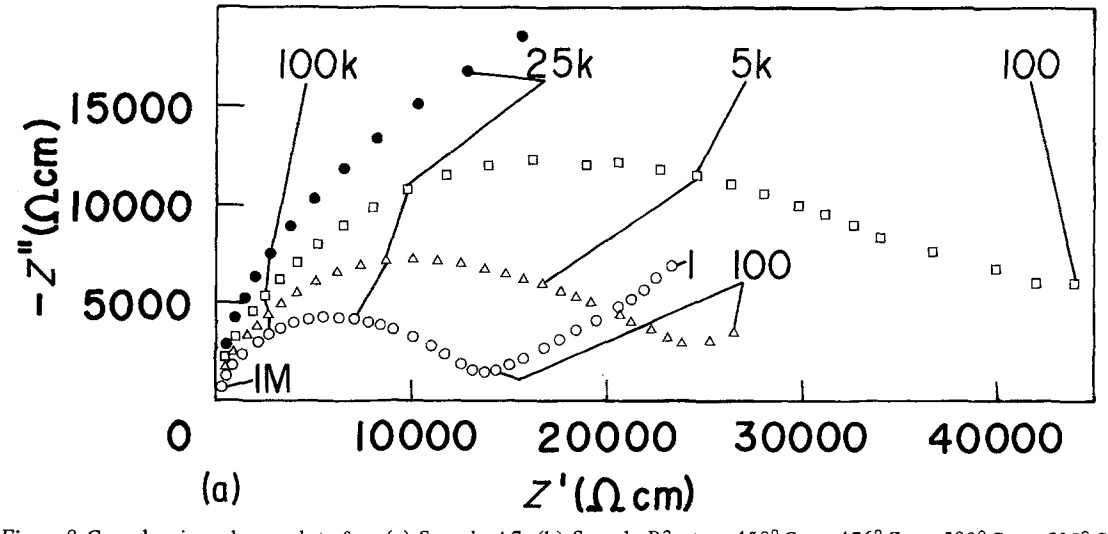

Figure 8 Complex impedance plots for: (a) Sample A7, (b) Sample B3 at •–450° C, □–476° C, △–500° C, ○–525° C. Frequencies are in Hz.

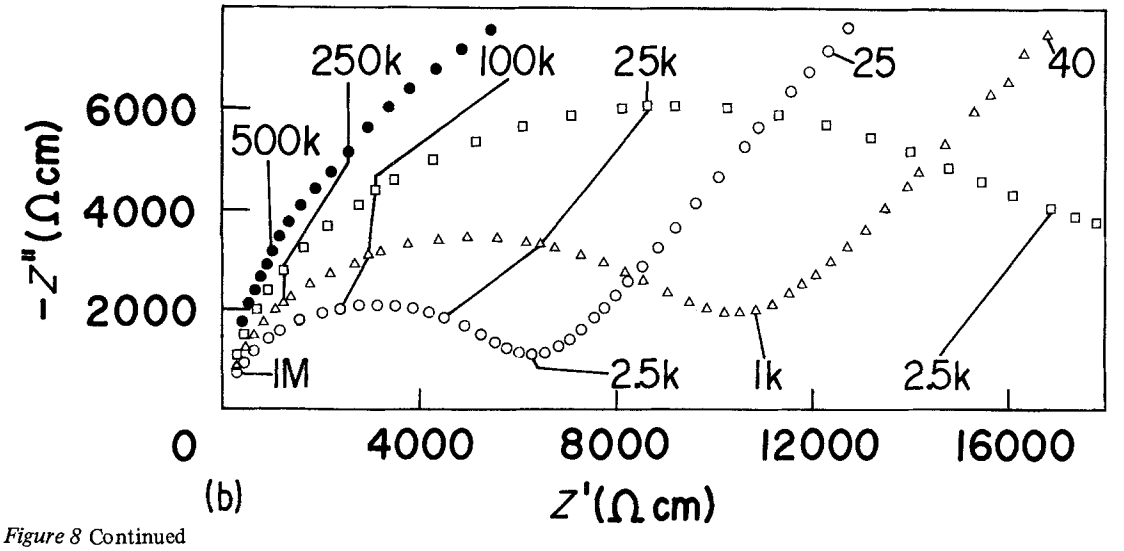

Figure 8 Continued

The Arrhenius conductivity plots showed a decrease in the activation energy with increase in temperature. The behaviour suggested the presence of two conducting processes in series, each with a different activation energy. The lower activation energy process, dominant at higher temperatures, is the bulk diffusion of oxygen ion vacancies. The higher activation energy process has not been identified. Complex impedance measurements at lower temperatures indicate a wide distribution of relaxation times confirming the presence of more than one conduction process.

Acknowledgements

The author wishes to express his gratitude to Dr M. J. Bannister for his constant interest, encouragement, many valuable discussions and critical review of this manuscript. The author also wishes to thank Mr F. T. Ciacchi for his assistance with many experiments and Mr R. K. Stringer for carrying out the heat treatments on some samples above 1700° C.

References

1. "Metal-Slag-Gas Reactions and Processes", edited by Z. A. Foroulis and W. W. Smeltzer (The Electrochemical Society Inc., Princeton, NJ, 1975).
2. "Measurements of Oxygen, Procedings of the Interdisciplinary Symposium", edited by H. Degn, I. Balslev and R. Brook (Elsevier, Amsterdam, 1976).
3. T. H. ETSELL and S. N. FLENGAS, *Metall. Trans.* 3 (1972) 27.
4. S. P. S. BADWAL, M. J. BANNISTER, F. T. CIACCHI and W. G. GARRETT, Proceedings of the 10th Australian Ceramic Society Conference, (The Australian Ceramic Society, Melbourne, Australia, 1982) p. 330.
5. M. J. BANNISTER, W. G. GARRETT, K. A. JOHNSTON, N. A. McKINNON, R. K. STRINGER and H. S. KANOST, in "Materials Science Monograph", Vol. 6, edited by P. Vincenzini (Elsevier, Amsterdam, 1980) p. 211.
6. W. G. GARRETT, Proceedings of the 10th Australian Ceramic Society Conference (The Australian Ceramic Society, Melbourne, Australia, 1982) p. 339.
7. D. W. STRICKLER and W. G. CARLSON, *J. Amer. Ceram. Soc.* 48 (1965) 286.
8. F. M. SPIRIDONOV, L. N. POPOVA and R. Ya. POPIL'SKII, *J. Solid State Chem.* 2 (1970) 430.
9. Z. S. VOLCHENKOVA and V. M. NEDOPEKIN, *Izv. Akad. Nauk. SSSR Neorg. Mater.* 10 (1974) 1821.
10. Z. S. VOLCHENKOVA, V. M. NEDOPEKIN, V. P. GORELOV and S. F. PAL'GUEV, *Izv. Akad. Nauk. SSSR Neorg. Mater.* 11 (1975) 1424.
11. L. S. ALEKSEENKO, A. M. GAVRISH, N. V. GUL'KO, G. P. OREKHOVA, L. A. TARASOVA and N. P. POLNITSKAYA, *Russ. J. Inorg. Chem.* 26 (1981) 476.
12. S. P. S. BADWAL, *J. Aust. Ceram. Soc.* 18 (1982) 35.
13. S. P. S. BADWAL, *J. Mater. Sci.* 18 (1983) 3117.
14. R. C. GARVIE and P. S. NICHOLSON, *J. Amer. Ceram. Soc.* 55 (1972) 303.
15. M. J. BANNISTER and P. SKILTON, *J. Mater. Sci. Lett.* to be published.
16. J. M. WIMMER, H. C. GRAHAM and N. M. TALLAN, in "Electrical Conductivity in Ceramics and Glass" Part B, edited by N. M. Tallan (Marcel Dekker Inc., New York, 1974) p. 619.
17. R. B. GREKILA and T. Y. TIEN, *J. Amer. Ceram. Soc.* 48 (1965) 22.
18. W. I. ARCHER and R. D. ARMSTRONG, in "Electrochemistry", Vol. 7 (The Chemical Society, London, 1980) p. 157.

19. C. K. CHIANG, J. R. BETHIN, A. L. DRAGOO, A. D. FRANKLIN and K. F. YOUNG, *J. Electrochem. Soc.* **129** (1982) 2113.
20. J. S. COLE and R. H. COLE, *J. Chem. Phys.* **9** (1941) 341.

Received 14 February
and accepted 24 February 1983